Biosynthesized (SnO2/ZnO/TiO2) Composite for Gas Sensor Application: Structural and Sensing Performance Evaluation

Mohamed Ahmed¹, Taoufik Soltani²

¹Department of Physics, College of Science, University of Sumer, Iraq, Mohamed.ahmed@uos.edu.iq ²Université de Tunis El Manar, Faculté des Sciences de Tunis, Laboratoire de Physique de la Matière Molle et Mécanique de fluide (LR99ES16), 2092 Tunis, Tunisia

presents study a green synthesis approach for the preparation of a nanocomposite, incorporating zinc oxide (ZnO), titanium oxide (TiO2), and tin oxide (SnO2). The process involves utilizing sweet potato-extracted solution as a reducing agent. The preparation of materials begins with the creation of a sweet potato-extracted solution, and subsequent synthesis of SnO2-ZnO-TiO2 films by mixing ZnO, TiO2, and SnO2 precursors. The resulting films are subjected to various processing steps, including precipitation collection, washing, and thin film formation. The sensor characteristics of the synthesized films are investigated by evaluating their resistance in the presence of NO2 gas at different operating temperatures. The observed resistance trends are discussed concerning the semiconductor nature of the films and temperature-dependent physisorption and chemisorption processes. The addition of ZnO and TiO2 to SnO2 enhances sensitivity to NO2, attributed to surface modification, synergistic effects, band structure tuning, and improved gas adsorption. The nanocomposite's structural, morphological, and optical characteristics are analyzed using X-ray diffraction (XRD). Structural properties for ZnO, TiO2, and SnO2 nanoparticles (NPs) are presented, including crystallite size calculations. The results indicate distinct crystalline structures for each oxide. The green-synthesized nanocomposite (ZnO: TiO2: SnO2) exhibits XRD patterns consistent with the individual oxide phases. This research underscores the potential of utilizing sweet potato-extracted solution in green synthesis methods, showcasing the environmentally friendly approach for fabricating multifunctional nanocomposites. Further validation and comparison with established methods are suggested to ensure reliable results. The demonstrated structural and sensor characteristics provide valuable insights for potential applications in electronic and sensing technologies.

Keywords: Green Synthesis, Nanocomposite Sensors, Sweet Potato Extract.

1. Introduction

Advancements in technologies facilitating the digital dissemination of environmental

information necessitate the ongoing refinement of functional electronic components and sensors. Gas sensors, solar- and photocells, as well as photocatalysts, play a pivotal role in this progression, relying predominantly on semiconductor-based materials. Within the domain of gas sensors, there is a noteworthy focus on synthesizing and investigating the properties of oxide materials composed of diverse elements to optimize sensor performance [1]. The most commonly used materials in cost-effective commercial sensors encompass zinc oxide, tin dioxide, indium oxide, and titanium dioxide. These materials are characterized by favorable traits, including chemical stability, non-toxicity, and a robust chemo-resistive response to a variety of gases. Such attributes make them appealing to both societal and industrial interests[2]. Zinc oxide and tin dioxide, in particular, emerge as extensively researched oxides, having pioneered their application as gas sensors. SnO2 and ZnO, distinguished by a wide band gap ranging from approximately 3 to 3.37 eV at room temperature and n-type conductivity, offer the flexibility to introduce impurities or heterojunctions, allowing for precise tuning of their gas-sensitive properties [3, 4].

In recent research, significant attention has been directed towards nanocomposite materials comprised of varying ratios of ZnO and SnO2 oxides, owing to their exceptional gas-sensitive properties [5]. These nanocomposites are commonly synthesized through hydrothermal processes, chemical technologies, electrospinning, atomic layer deposition, magnetron evaporation, spray pyrolysis, among others[4]. The formation of a two-phase structure involving ZnO and SnO2 oxides is attributed to relatively low annealing temperatures (<600 °C), as theoretically demonstrated. Temperature treatment is instrumental in fine-tuning the functional properties of these oxides [6].

Exploring the optical properties of ZnO-SnO2 composite films synthesized via magnetron sputtering revealed a band gap within the range of 3.3–3.32 eV, dependent on the specific technological protocols employed. The concentration of tin ions plays a critical role as a modifying additive for the composite materials[6]. For instance, in the synthesis of SnO2-ZnO films using spray pyrolysis, it was observed that a maximum Sn ion concentration of around 8% is ideal for maintaining crystal properties. Exceeding this concentration to 10% can result in a deterioration of composite properties. Additionally, an increase in Sn ion concentration up to 6% leads to a narrowing of the band gap to 2.72 eV [7].

Enhancements in sensor properties within nanocomposite materials are attributed to alterations in surface oxygen forms and the synergistic effect of forming n—n heterojunctions, resulting in the creation of potential barriers. Notably, the incorporation of small concentrations of Sn4+ into zinc oxide has been shown to improve gas sensitivity to NO2. Gas response studies on materials with a Sn:Zn ratio of 5:87, obtained through chemical technologies, demonstrated a substantial gas response at 146 $\,^{\circ}$ C when exposed to 1 ppm of NO2. Similarly, gas sensors based on materials with a Sn:Zn ratio of 5:85 exhibited a significant gas response at 88 $\,^{\circ}$ C with exposure to 0.55 ppm of NO2 [8] [9].

This brief literature overview underscores the critical role of varying Sn content in ZnO-SnO2 films for tuning their gas-sensing properties, emphasizing the need for precise technology protocols. While approaches like sol–gel methods and hydrothermal synthesis may have limitations in terms of time or equipment cost, the study posits that a green-synthesis method involving plant-extracted SnO2 and ZnO nanoparticles, applied through Spin coting and

chemical bath deposition, may present a simple and economically viable alternative for systematic exploration [10] [11]. The current study aims to investigate the impact of SnO2 additives in ZnO films with a 1:1 ratio synthesized using spin coting method technique.

2. Materials and Methods

Materials

Zinc ,Tin and titanium precursor (Zinc chloride , Tin chloride and titanium chloride), Zinc chloride tetrahydrate (sigma Aldrich), Deionized distilled water (DDW), Tin (IV) chloride, pentahydrate (sigma Aldrich) Titanium (III) chloride solution (sigma Aldrich)

, sweet potato Extracted, Glassware and laboratory equipment (beakers, stirrers, etc.).

Preparation of Materials

Preparation of sweet potato Extracted Solution

In a separate clean beaker, prepare a solution of sweet potato Extracted by accurately measuring the desired amount 200 gm of sweet potato cute to small pieces Add an appropriate volume of deionized water to the beaker has the 200 gm of sweet potato, in 600 ml of water. ensuring a suitable concentration of the sweet potato solution. Keep the mixture thoroughly for 12h in 20 Co.

Synthesis of Tin Oxide, Zinc Oxide

This laboratory method presents a green synthesis approach for the preparation of 1:1 mixing tin oxide (SnO2) Zinc oxide (ZnO) and titanium oxide (TiO2), nanoparticles using sweet potato Extracted as a reducing agent For SnO2-ZnO, 0.5M of Zinc chloride in 100 ml DWW was mixed with 0.5 M of Tin chloride and 0.5M of titanium chloride in the same beaker and stirred in 50 Co for 30 Min stirring then added the sweet potato Extracted about 40 ml solution for the beaker. any color changes or formation of precipitates, indicating the progress of the reduction reaction. stirring continues for an appropriate duration of 30 min to allow the reduction reaction to occur fully.

Precipitate Collection

Upon concluding the reaction, retrieve any formed precipitate through centrifugation at 4500 rpm for 15 minutes. Transfer the gathered precipitate to a pristine container for subsequent processing. Perform a thorough washing of the precipitate using deionized distilled water (DDW), collecting any resulting precipitate through centrifugation at 4500 rpm for 15 minutes. Iterate the washing procedure until the precipitate appears devoid of contaminants.

In zinc oxide and tin oxide film preparation, dispensing is key, with static (depositing fluid at the center) and dynamic (dispensing during substrate rotation) methods. Static dispense volume (1-10 cc) depends on fluid viscosity and substrate size. Dynamic dispense, at 500 rpm, minimizes waste. The choice influences film uniformity, requiring understanding of fluid properties, substrate size, and coverage needs. Subsequent spinning and drying contribute to high-quality films for electronics and sensing applications.

Drying and Calcination of the Precipitate thin films:

Dry the precipitate (containing Zinc Oxide and Tin Oxide Titanium Oxide) using either airdrying or low-temperature oven drying (e.g., at 60°C). Afterward, subject the samples to calcination at temperatures up to 500 degrees Celsius until all moisture is eliminated. This method presents a green synthesis approach for Zinc Oxide , Tin Oxide and titanium oxide (SnO2:ZnO/TiO2) using sweet potato as a reducing agent, highlighting its potential as an environmentally friendly strategy. Further validation and comparison with established methods are crucial to ensure reliable results, given the experimental nature of this modified procedure.

3. Results and discussion

Structural, Morphological, and Optical Characteristics

The green-synthesized NPs/NCs were structurally characterized using X-ray diffraction (XRD). Table (3) provides structural properties for ZnO, TiO2, and SnO2 NPs, while Figures (3-1), (3-2), and (3-3) depict their respective XRD patterns.

For ZnO NPs, the strongest diffraction peaks at 2-theta values of 31.811, 34.481, and 36.307 correspond to (100), (002), and (101) miller indices, consistent with the hexagonal (Wurtzitephase) structure (COD card number 96-230-0451). The average crystallite size is determined as 16.411 nm [12]. In TiO2 NPs, prominent peaks at 2-theta values of 25.16, 37.359, and 47.635 align with (011), (004), and (020) miller indices, confirming a tetragonal (Anatasephase) structure (COD card number 96-900-8217). The average crystallite size is calculated as 22.687 nm [13]. For SnO₂ NPs, the strongest peaks at 2-theta values of 27.09, 34.37, and 52.23 correspond to (110), (101), and (211) miller indices, indicating a cubic structure (COD card number (96-10-0063). The average crystallite size is determined as 21.75 nm [14].

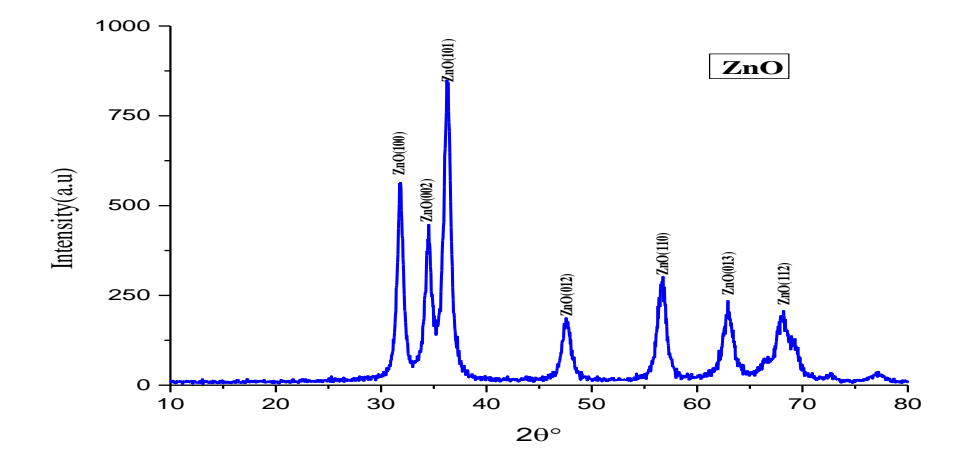


Figure 1 XRD pattern of ZnO NPs

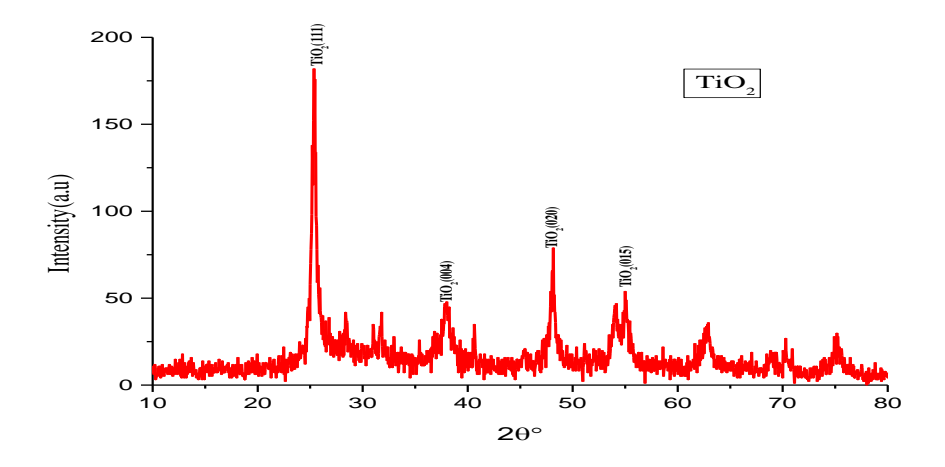


Figure 2 XRD pattern of TiO₂ NPs

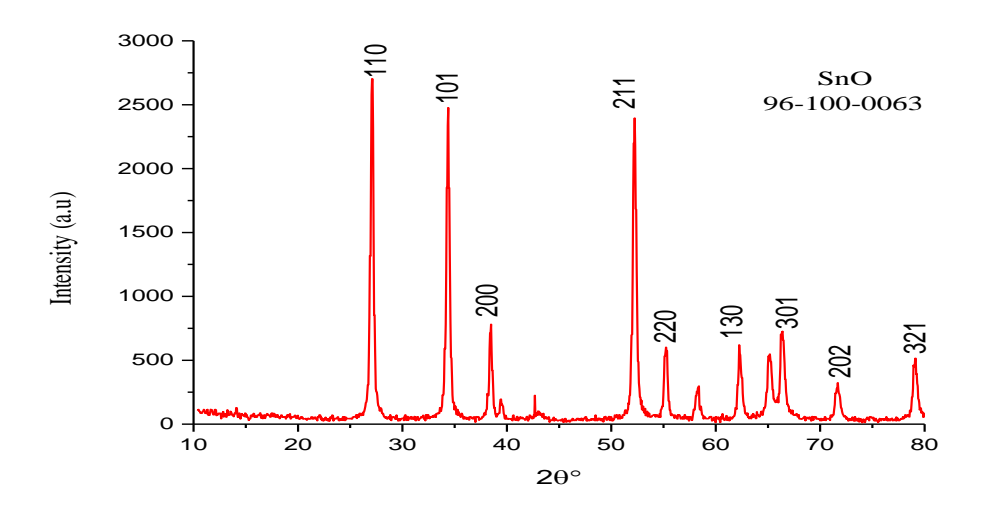


Figure 3 XRD pattern of SnO2 NPs.

Table 1 Structural properties of ZnO, TiO2, and SnO2 NPs

Sample	ZnO NPs		TiO ₂ NPs		SnO ₂ NPs				
Τωο θ	Strongest three peaks		Strongest three peaks		Strongest three peaks				
(Deg.)	31.811	34.481	36.307	25.16	37.36	47.635	27.09	34.37	52.23
hkl	100	002	101	011	004	020	110	101	211
FWHM (Deg.)	0.434	0.556	0.636	0.2826	0.4065	0.552	0.36	0.39	0.42
Crystallite size (nm)	19.879	15.625	13.729	30.083	21.547	16.431	22.78	21.31	21.16
Average Crystallite size (nm)	16.411			22.687		21.75			
Entry.	9	96-230-045	1	9	96-900-821	7	9	96-10-006	3
COD	(Hexagonal)		(tetragonal)		(cubic)SnO ₂				
СОВ	""	wurtzite"Zr	ıO	TiO ₂ "Anatase"					

Table (1-2) gives the structural properties of nanocomposite , and Figure (4) shows the X-ray diffraction patterns of the green synthesized (ZnO: TiO2: SnO2) nanocomposite. All the strongest diffraction peaks patterns of the nanocomposites most substantial through 2theta can be well-matched with the miller indices (hkl) . The resultant data structure is well-matched with the (COD) cards number (96-900-8217) (tetragonal- structure) of TiO2 in the Anatase phase, (96-100-0063) (monoclinic- structure) of SnO2, and (96-230-0451) (hexagonal-structure) of ZnO; all these structures are forming (ZnO: TiO2: SnO2) nanocomposite with an average crystallite size of 21.99 nm.

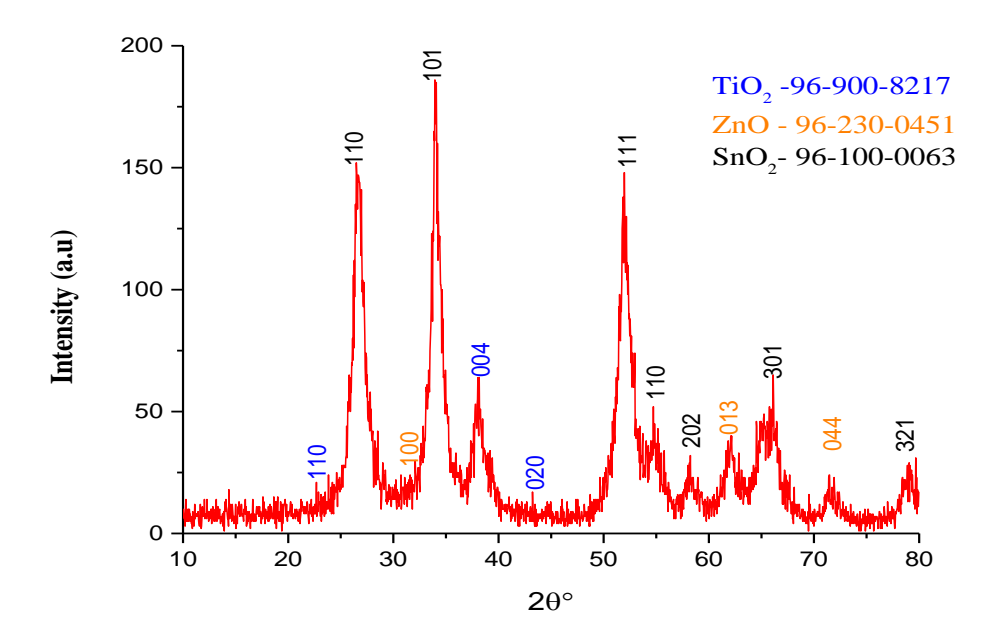


Figure 3 XRD pattern of (ZnO: TiO2: SnO2) Nanocomposite

Table 2 Structural properties of (ZnO: TiO₂: SnO₂) Nanocomposite

	N	anocomposite		
2θ (Deg.)	FWHM (Deg.)	hkl	Crystallite Size nm	Average crystallite size nm
26.71	0.36	110	22.76	
34.08	0.39	101	21.29	
38.06	0.34	004	24.86	
52.00	0.42	111	21.14	21.99
54.60	0.37	110	24.12	21.99
58.30	0.41	202	22.30	
62.07	0.45	013	20.78	
65.59	0.47	301	19.90	
79.06	0.50	321	20.72	

Figure 4 show exhibiting unique properties. To understand the structure of such nanocomposites, X-ray diffraction (XRD) is employed. XRD is a technique that analyzes how X-rays scatter when interacting with a sample, providing insights into the material's arrangement. In the context of crystallography, Miller indices are utilized to uniquely label crystal planes within a crystal lattice, aiding in the characterization of the material's structure. To support XRD analysis, Crystallography Open Database (COD) cards serve as reference databases. These cards house information essential for identifying crystal structures in materials like TiO2, SnO2, and ZnO. The materials (TiO2, SnO2, ZnO) can exhibit different crystal structures, such as the Anatase phase, monoclinic structure, and hexagonal structure. These structures influence the properties of the nanocomposite. One crucial aspect assessed through XRD is the crystallite size, representing the dimensions of individual crystals or grains within the material at the nanoscale. The combination of nanocomposite formation, XRD analysis, Miller indices, COD cards, and an understanding of crystal structures collectively contributes to a comprehensive scientific explanation of the material's composition and characteristics.

Scanning electron microscope (SEM) is a very powerful tool to characterize nanostructure and nanomaterial due to its high resolution and speed in directly measuring the nanoparticle's dimensions and shapes The Field emission scanning electron microscopy for SnO2, ZnO, TiO2 and SnO2-ZnO -TiO2

Figure 5. shows the FE-SEM image of SnO2 NPs prepared by green synthesis with an average size of about 35 nm and have spheroidal particle shape but with a growth process accompanied by agglomeration of SnO2 particles, which appears in Figure 5 as bright regions [15]. Assembly disease due to the finite size of nanoparticles with a growth rate distributed on all sides of the sample

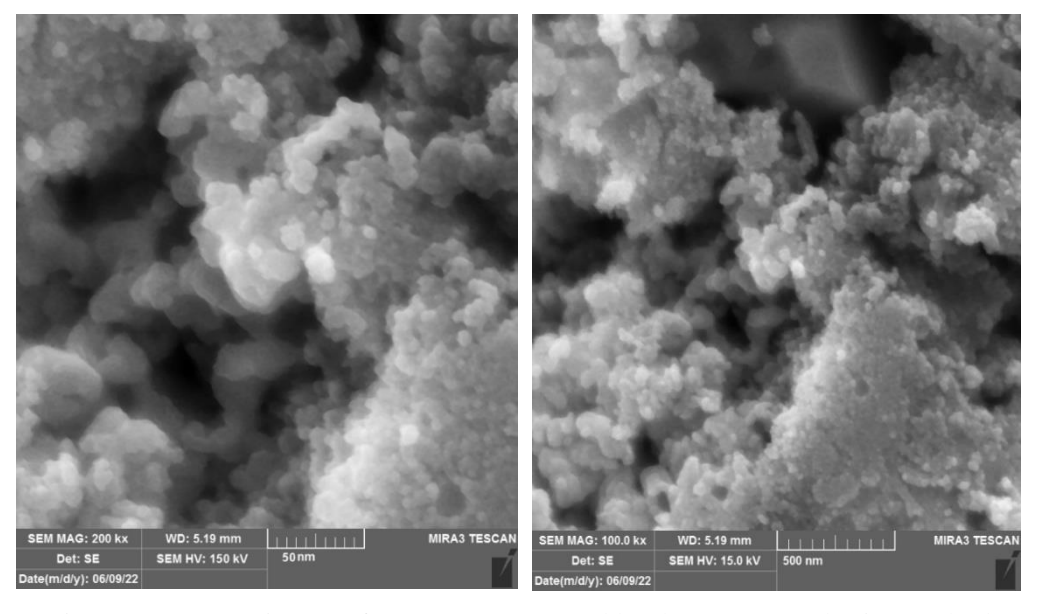


Figure 5 FE-SEM image of SnO2 NPs prepared by the Green synthesise method

Figure 6. shows the FE-SEM image of TiO2 NPs prepared by green synthesis with an average size of about 36 nm have Anatase (tetragonal) growth particle shape Which distinguishes the Anatase (tetragonal) TiO2 The change of shape has a wide effect on the change of physical properties in terms of area to unit volume, as well as chemical properties in terms of the surface area of the reactant. notice from Figure 1-6. that the surface area has increased to a unit volume

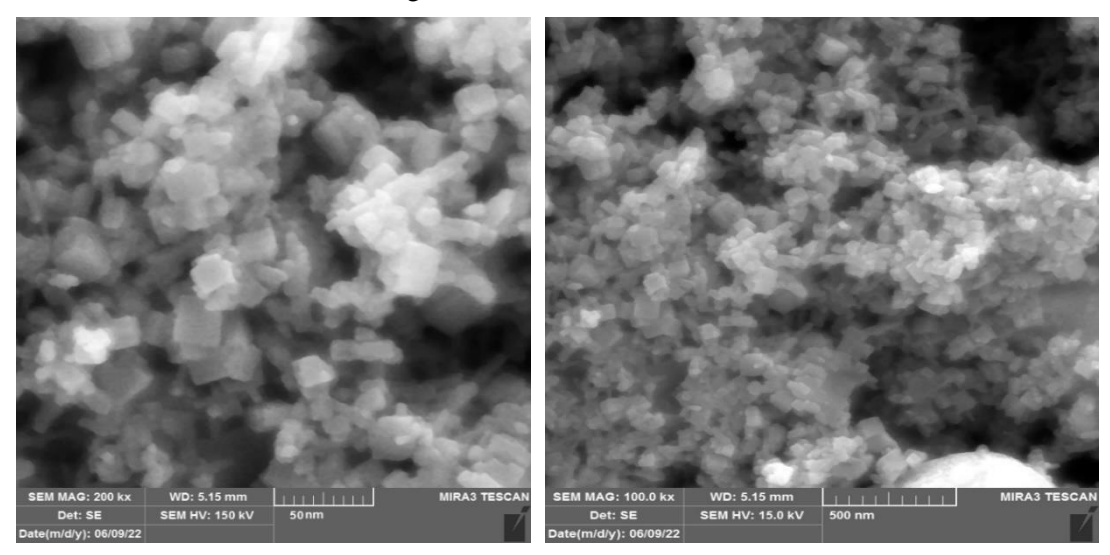


Figure 6 FE-SEM image of TiO2 NPs prepared by the Green synthesise method

Figure (7) shows that the prepared ZnO powder sample, which was synthesized green method, consists of rod-like microstructures with a relatively smooth and uniform surface of 200-300 nm in length and hexagonal cross-section with a diameter 66 nm.

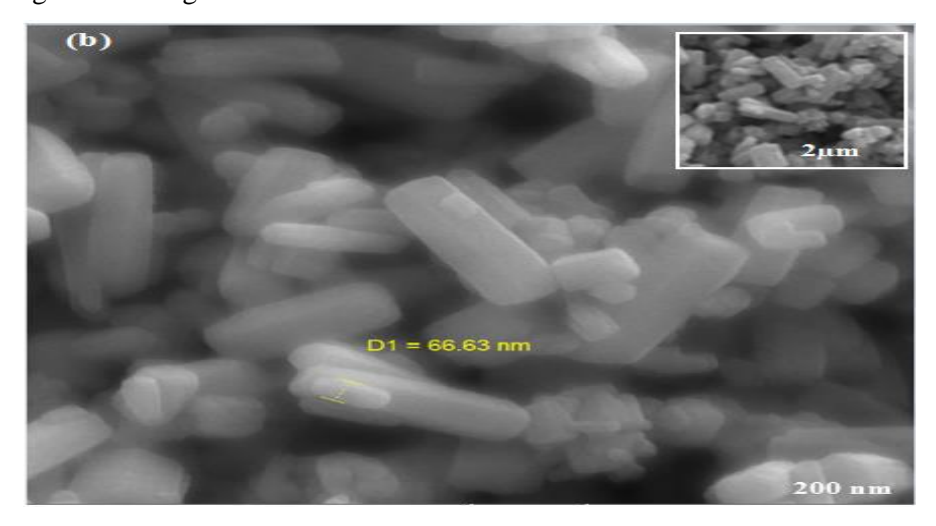


Figure 7: FE-SEM image of TiO2 NPs prepared by the Green synthesise method

In this case, the observed hexagonal cross-section and the specific dimensions of the rod-like structures indicate a well-controlled and reproducible synthesis process. Factors such as

reaction conditions, temperature, concentration of reactants, and the presence of specific organic molecules or plant extracts, commonly used in green synthesis, can contribute to the formation of these distinct microstructures.

Figure 8. shows the FE-SEM image of SnO2 - ZnO - TiO2 NPs prepared by green synthesis with an average size of about 35 nm and spherical particle shape The shape of the spheroidal growth is clearly distinguished and the growth distribution is spread across the sample in a consistent manner

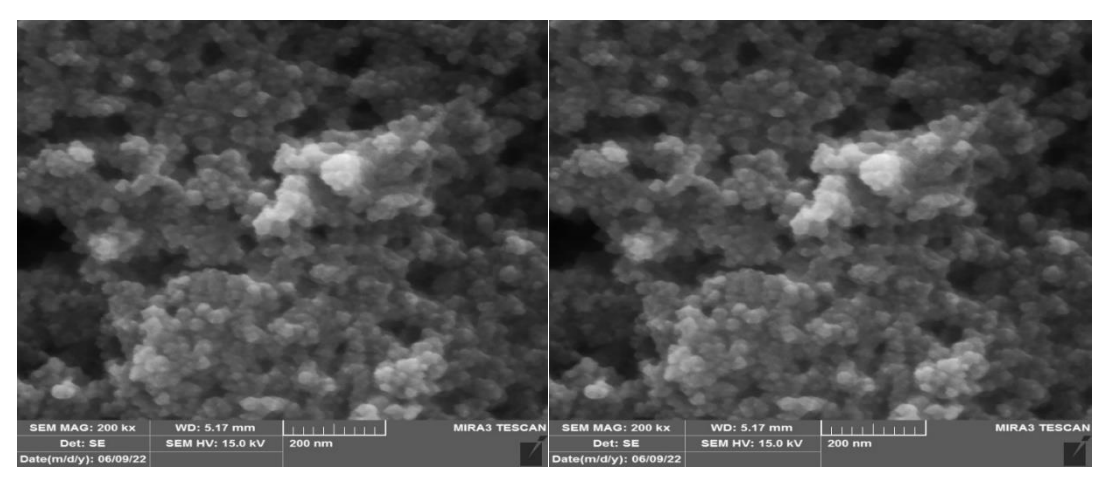


Figure 8 SnO2 - ZnO - TiO2 was prepared by the Green synthesise method

The absorbance measurements were calculated for colloidal nanoparticles using (UV-Spectroscopy). Figure 9. Indicates the absorption spectrum of SnO2, which falls within the low-wavelength range characterized by high-energy of UV, extend from 200 nm to 350 nm. indicating its ability to absorb high-energy blue colors.

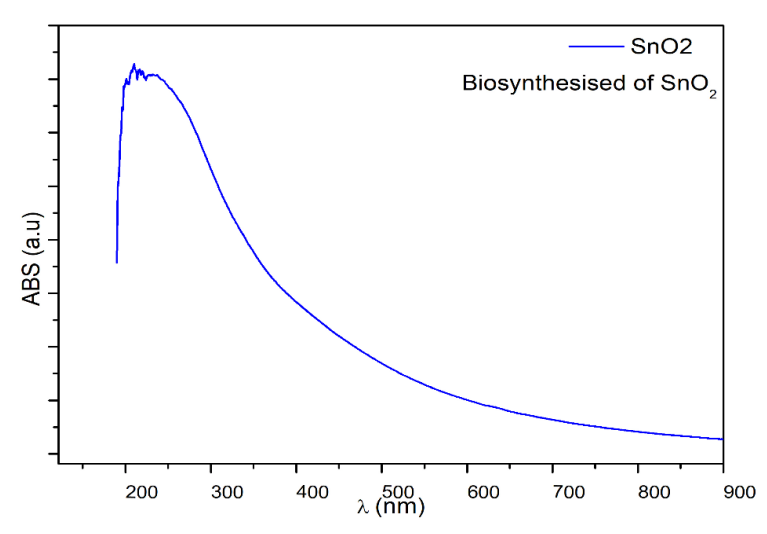


Figure 9 UV-Visible absorbance of SnO2 NPs prepared by Green synthesise method

Figure 10 The absorbance spectrum of Zinc oxide (ZnO), covers a broad range from 240 nm to 450 nm. This means that Zinc oxide nanoparticles are capable of absorbing light across this wavelength range. The breadth of this absorption spectrum indicates that Zinc oxide nanoparticles can interact with a wide range of light energies, making them versatile for various applications.

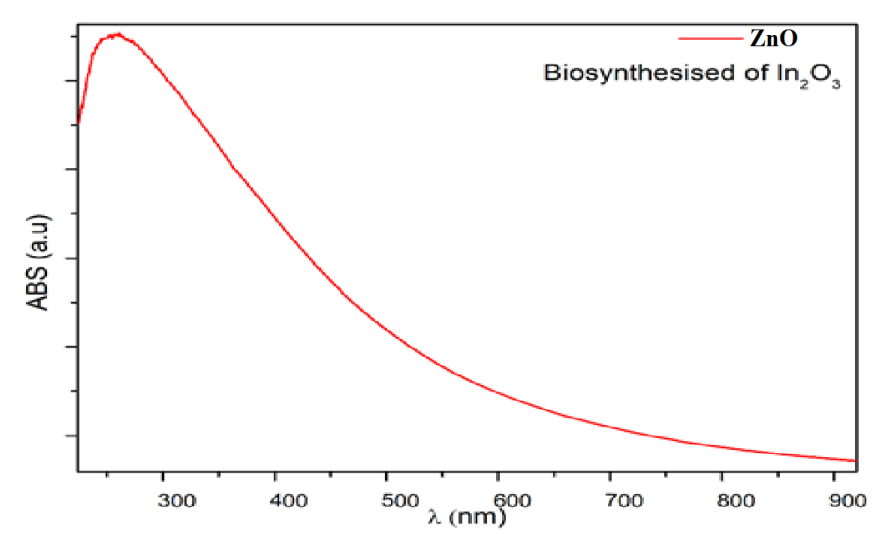


Figure 10 UV-Visible absorbance of In2O3 NPs prepared by Green synthesise method

Figure 11. shows the absorbance of TiO_2 , which is within the range of low wavelengths with high energy blue colours .The relationship between increased absorbancy and volume for TiO_2 , particularly in the low-wavelength range of 200 nm to 380 nm where it absorbs high-energy blue light, changes in the volume of TiO_2 impact its absorbancy within the mentioned wavelength range.

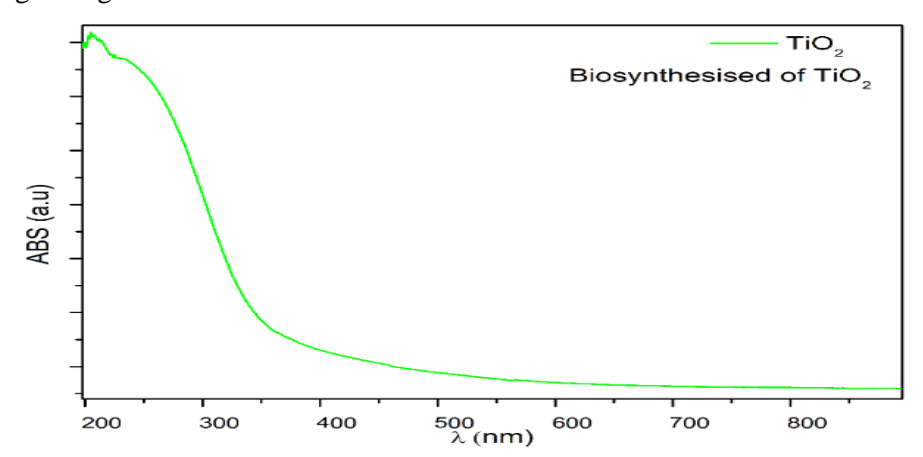


Figure 11 UV-Visible absorbance of TiO2 NPs prepared by Green synthesise method

Figure. 12 demonstrates the optimal absorption characteristics observed in SnO2-ZnO-TiO2 prepared through the Green synthesise method. the absorption range significantly widens

while maintaining consistent intensity levels, which are indicative of the density of the prepared nanoparticles. The absorption capacity extends broadly from 200 nm to 500 nm due to the overlap of sub-energy levels [15-17].

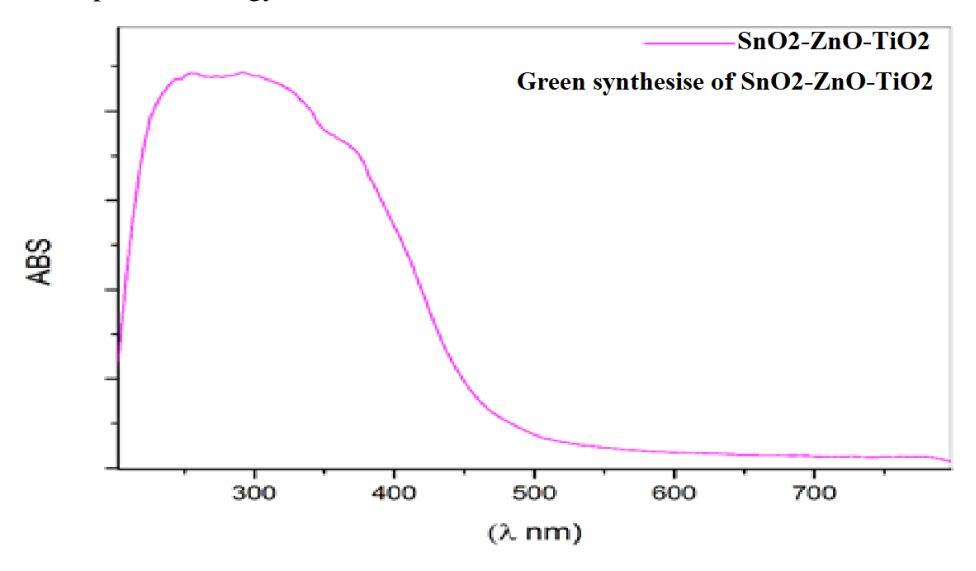


Figure 12 UV-Visible absorbance of SnO2-ZnO-TiO2 NPs prepared by Green synthesise method

The energy gap was calculated using the Tuce equation

$$\alpha(E) = A(E - E_g)^n$$

where: A is a constant proportional to the absorption coefficient E is the energy of the incident photon (hv) E_g is the optical bandgap energy n is an exponent that depends on the nature of the electronic transitions involved in the absorption process where the value of (r=1/2), and by plotting the relationship between (α hv)2 and (hv) by choosing the best tangent to the straight portion of the curve to cross the energy axis of the incident photons at the point (α hv)2, where it represents the energy band gap value of the optical transitions, This decrease in the energy gap is caused by an increase in the granular size of the precipitant material, which creates donor levels within the energy gap and near the conduction beam and thus increases the absorption of photons of less energy, and this is consistent with the results [17]

The energy gap was measured for three samples of SnO2-ZnO-TiO2 in Figure 1-13, which are prepared by the Green synthesize Figure 1-13 shows the energy band gap for the ZnO, TiO2, and SnO2 was Eg=3.34 eV, 3.5eV and 3.1 eV respectively

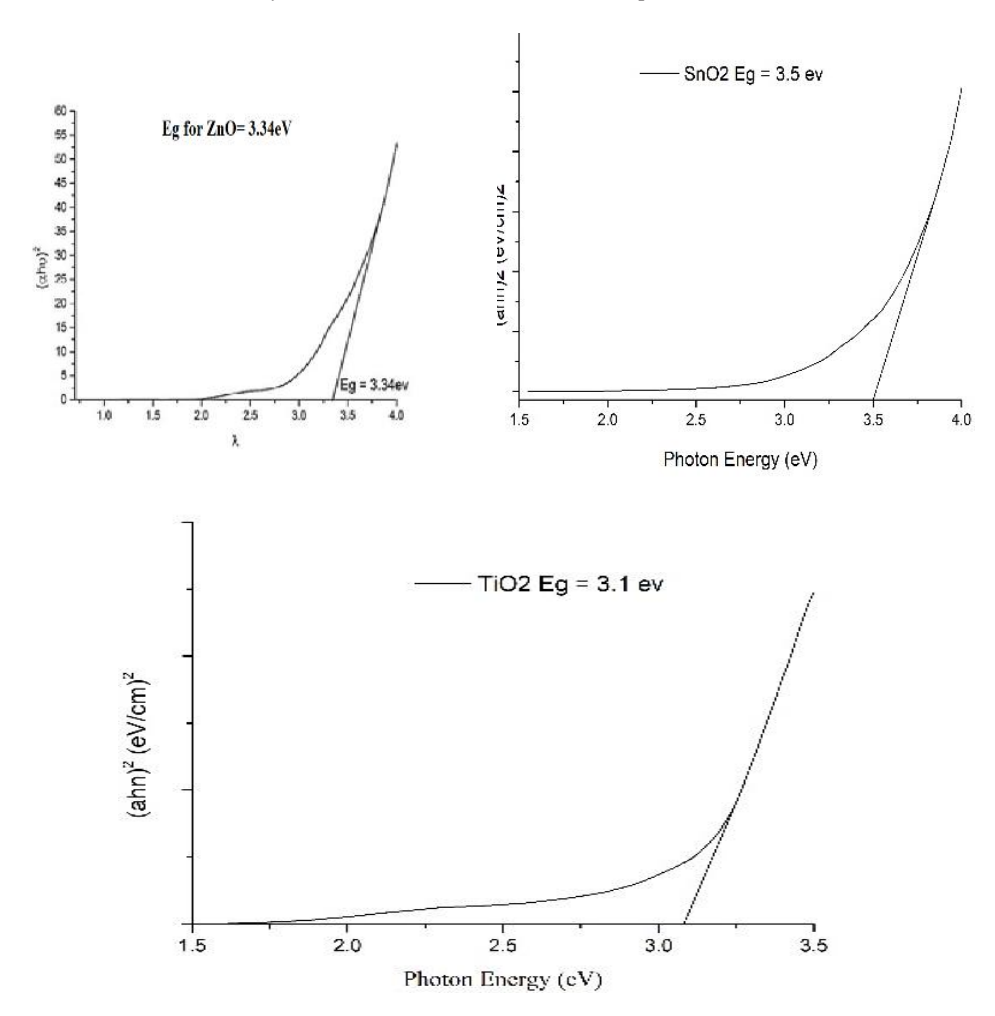


Figure 13: Optical energy gap of the ZnO, SnO2 and TiO2 prepared by the green Synthesis method

Figure 14. shows the reveals crucial insights. As the tangent line intersects the x-axis at Photon Energy (eV), distinct energy band gaps emerge at 2 eV and 2.4 eV for SnO2-ZnO-TiO2. three specific energy gaps at 2.7 eV, 2.4 eV, and 2 eV point to the core-shell nature of the nanoparticles. The prevalence of several direct energy gaps indicates the dominance of this state in the composite nanoparticles synthesized via the Biochemical method. This dominance arises from the overlapping of energy levels and the emergence of sub-levels during the chemical preparation, a bottom-up method relying on molar concentrations. The preparation strategy allows sufficient time for ions to gather as atoms and align sub-levels, establishing in the crystal lattice the prominence of the direct energy gap [18].

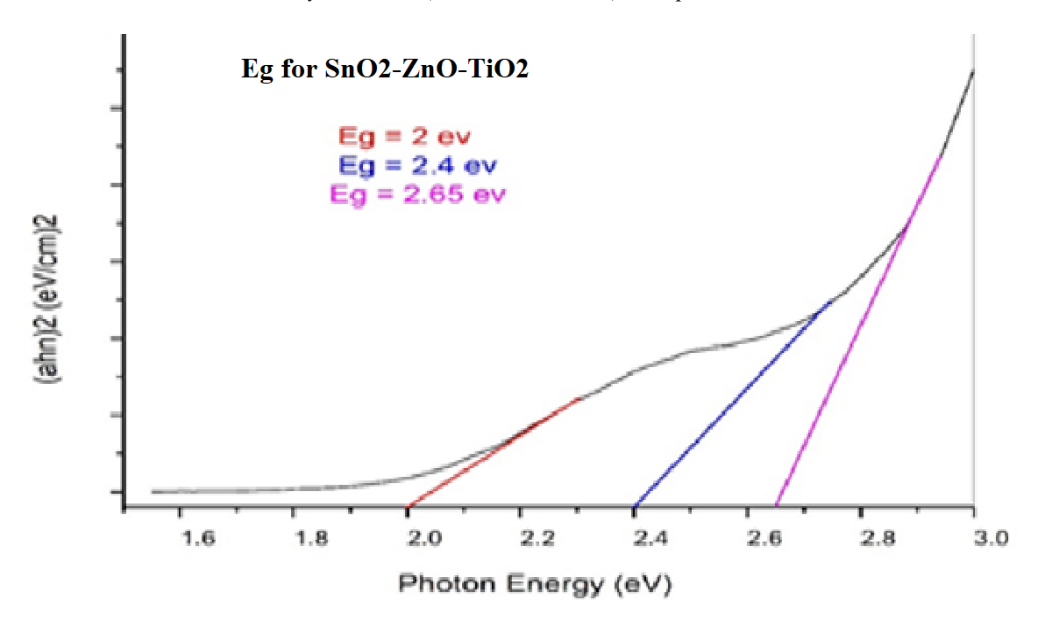


Figure 14: Optical energy gap of the SnO2-ZnO-TiO2 was prepared by the Biochemical method

EDS or EDX is an analytical method used to characterize a sample's chemical makeup or determine its elemental composition. The EDX technique was used in the current investigation to evaluate the NPs contents as well as any pollution that had been built up inside of them. Images from the EDX quantitative analysis of the samples are displayed in Figures 15, 16,17 and 18. The purity of the SnO2, ZnO, TiO2, and SnO2-ZnO-TiO2 are calcinated at 500°C for 2 hours respectively nanoparticles are confirmed Table 0-3,4, and 6 Quantitative results from EDX analysis for pure SnO2, ZnO, TiO2, and SnO2-ZnO-TiO2 NPs prepared and calcinated at 500°C for 2 hours [19]

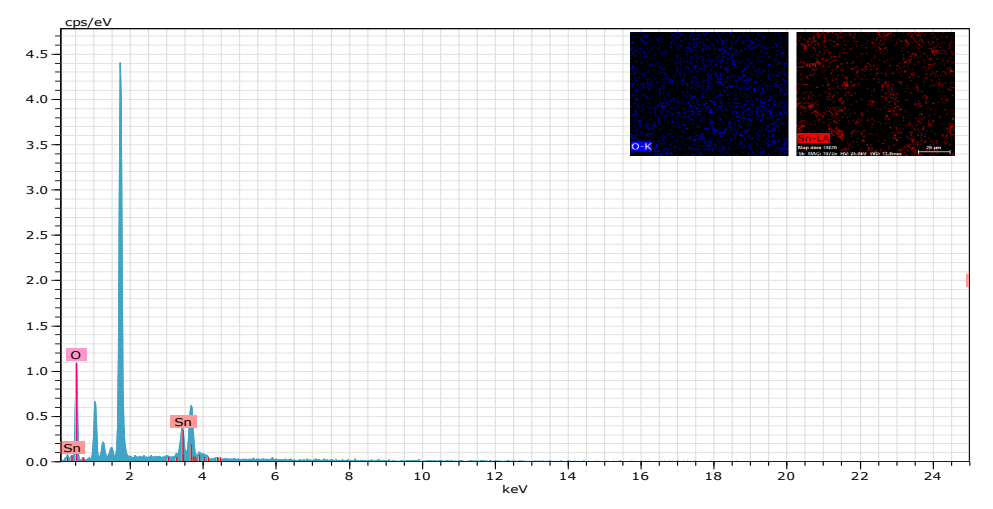


Figure 15 EDX results of pure SnO2 NPs prepared and calcinated at 500°C for 2 hours

Table 3 Quantitative results from EDX analysis for pure SnO2 NPs prepared and calcinated at 500°C for 2 hours

Element	Weight %	Atom %
Sn	73.89	95.45
0	26. 11	4.55
SUM	100	100

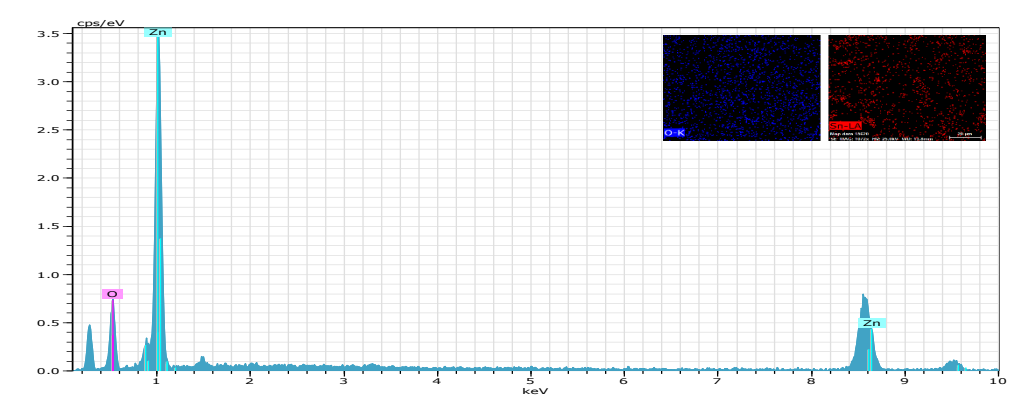


Figure 16 EDX results of pure ZnO NPs prepared and calcinated at 500°C for 2 hours

Table 4 Quantitative results from EDX analysis for pure ZnO

Element	Weight %	Atom %
Sn	73.89	95.45
0	26. 11	4.55
SUM	100	100

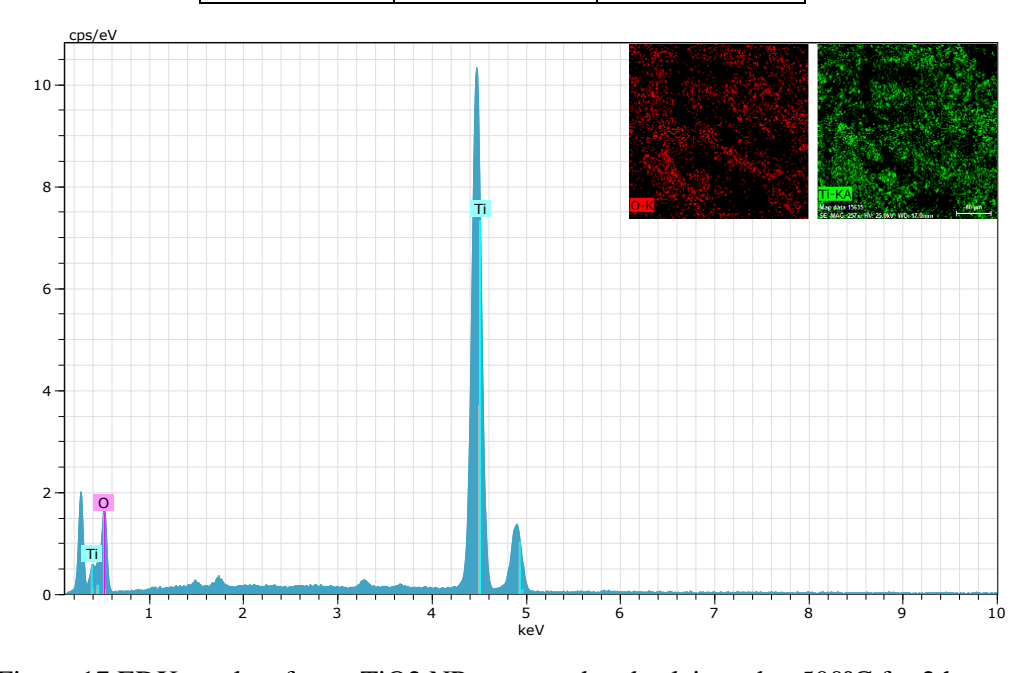


Figure 17 EDX results of pure TiO2 NPs prepared and calcinated at 500°C for 2 hours

Table 5 Quantitative results from EDX analysis for TiO2 NPs prepared and calcinated at 500°C for 2 hours

Element	Weight %	Atom %
Ti	70.32	87.64
0	29.68	12.36
SUM	100	100

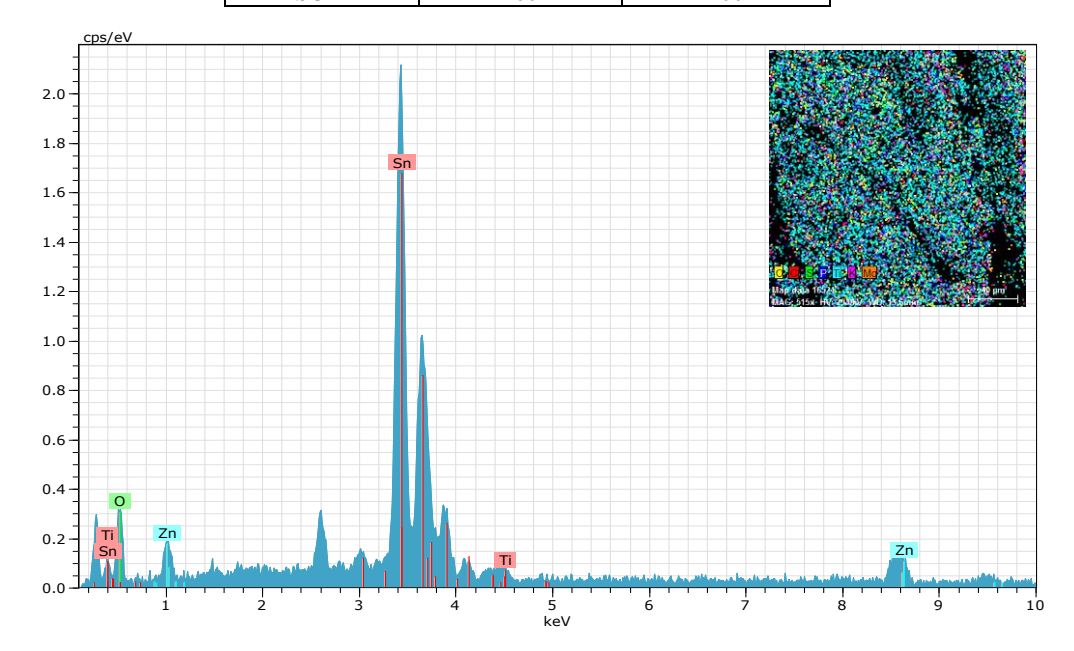


Figure 18 EDX results of pure SnO2-ZnO-TiO2 NPs prepared and calcinated at 500°C for 2 hours

Table 6 Quantitative results from EDX analysis for pure SnO2-ZnO-TiO2 NPs prepared and calcinated at 500°C for 2 hours

Element	Weight %	Atom %
Sn	67.52	25.71
0	24.04	67.92
Zn	6.34	4.38
Ti	2.10	1.99
SUM	100%	100%

To assess the sensor properties of SnO-ZnO-TiO films, synthesis and calcination were conducted at various temperatures, particularly at 500°C. The resistance of the films, deposited on different substrates at varying temperatures, was examined in the presence of NO2 gas. This evaluation was performed across different operating temperatures to study the film's response to the gas under different conditions.

As depicted in Figure (19), the resistance of SnO2, ZnO, TiO2, and SnO2-ZnO-TiO2 films demonstrates a consistent decrease with the rise in operating temperature before exposure to NO2 vapor. This behavior is characteristic of semiconductor materials, as reported in various metal oxides[6, 20].

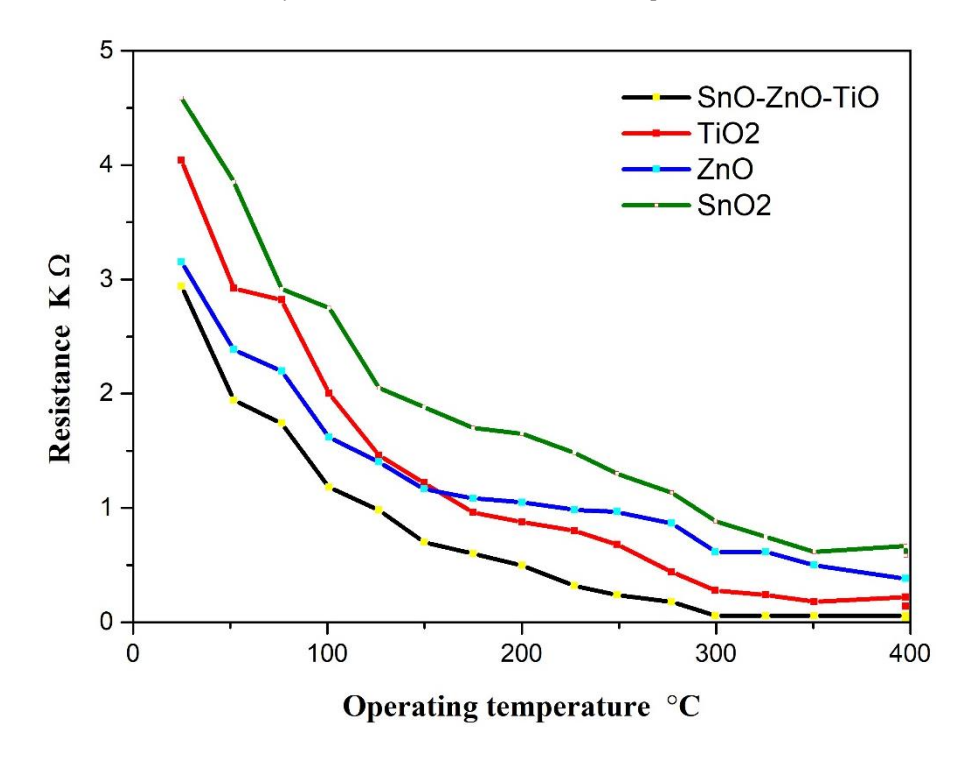


Figure 19 Resistance of SnO2, ZnO, TiO2, And SnO2-ZnO-TiO2 Films

The overall resistance behavior (Ra) can be categorized into three distinct temperature regions:

Low Temperature (i): At low temperatures, oxygen undergoes physisorption on the film's surface, capturing electrons from the interior. This results in an initial decrease in resistance.

Moderate Temperature (ii): At moderate temperatures, physisorbed oxygen species (O-) convert into chemisorbed oxygen (2O-), leading to a further reduction in Ra.

Higher Temperature (iii): At higher temperatures, Ra continues to decrease due to the semiconducting nature of the films.

The observed trend indicates that the resistance decreases with increasing substrate temperatures up to 400°C. However, beyond 400°C, a slight increase in film resistance occurs. This shift is attributed to the crystallinity of the films and the associated mobility of carriers.

Figure (20) show the variation of sensor resistance prepared at different substrate temperature as a function of operating temperature after exposed to the 20 ppm NO2 gas, it's clear that the resistance of all film's resistance decreases after exposed to NO2 gas, which due to the behaviour of NO2, it removes adsorbed O- species from the surface and reinjects the electron back into the material, thereby reducing the resistance. The released electrons in the process will increase the carrier concentration, making a thinner depletion layer; therefore, the electrical resistance of the ZnO will decrease and the conductivity will increase. Also shows the resistance decrease with increase substrate temperature up to 400°C and then slightly [20]

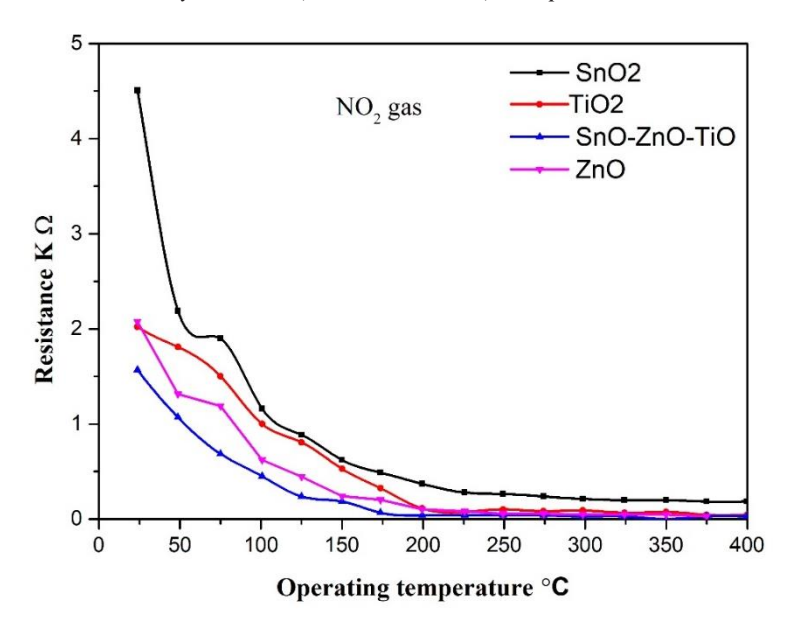


Figure 20 variation of sensor resistance prepared at different substrate temperature as a function of operating temperature

Figure. (21) shows the variation of sensitivity of the SnO2 sensor with operating temperature in the range (25–400°C). It is found that sensitivity of SnO2 films increases with increasing in operating temperature and shows maximum peak values at optimal temperature and then the sensitivity decreases with further increase in temperature. At the optimal temperature, the activation energy may be enough to complete the chemical reaction. The optimum working temperature was determined at 250 °C for all sensors [21],

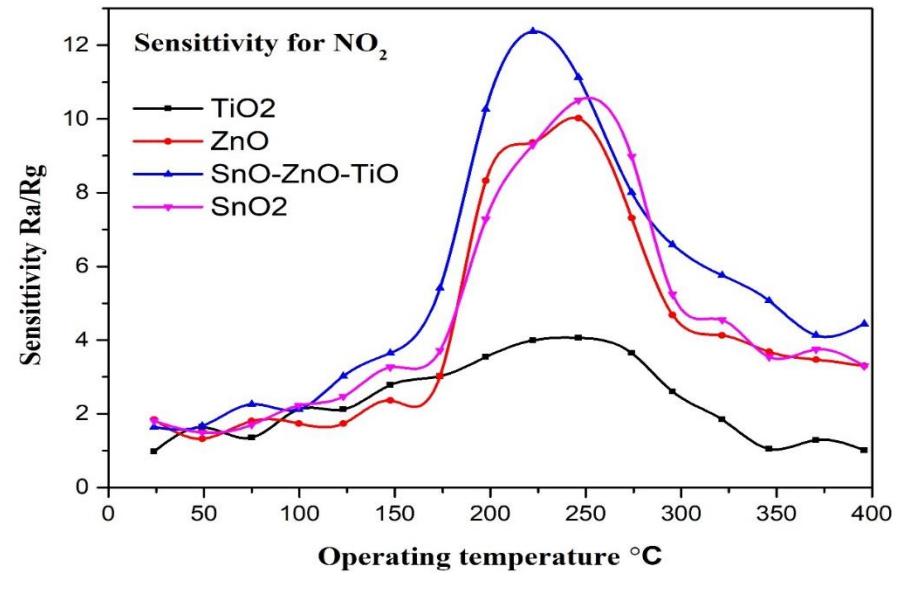


Figure 21 variation of sensitivity of the SnO2 sensor with operating temperature

Nanotechnology Perceptions Vol. 20 No. S4 (2024)

The resistance of the films, deposited on substrates was examined in the presence of NO2 gas. This evaluation was performed across different operating temperatures to study the film's response to the gas under different conditions. SnO-ZnO-TiO films prepared exhibit a maximum response at 225°C which is attributed to the decrease of defect of films which leads to an increase in mobility carriers. the addition of zinc oxide and titanium oxide to tin oxide enhances sensitivity to NO2 gas through surface modification, synergistic effects, band structure tuning, enhanced gas adsorption, and the optimization of the composite material composition. These factors contribute to an improved gas-sensing performance of the ternary oxide system[21-23]

TE 11 7 C1 1 1 1 1 1 1 1 1 1 1 1 1 1 1 1 1	. 11	
Table / Show the working	tamparatura and lawast ras	nonce fime and recovery fime
Table / Show the working	temperature and rowest res	ponse time and recovery time

Ts(°C)	Sensitivity	Response time s	Recovery time s
TiO2	4.4	59	87
ZnO	10.7	42	74
SnO-ZnO-TiO	13.3	36	69
SnO2	11.3	40	72

SnO-ZnO-TiO thin film was chosen to calculate the response time and recovery time as the thin film gives the best gas sensitivity. The results of response and recovery time at different substrate temperatures to determine the optimum working temperature and lowest response time and recovery time are Table 7 and show that the response time and the recovery time decrease when increase substrate temperature Figure. (22) shows that when the operating temperature increases both response time and recovery time decrease for SnO-ZnO-TiO thin film, the rise in temperature causes faster response and longer recovery times.

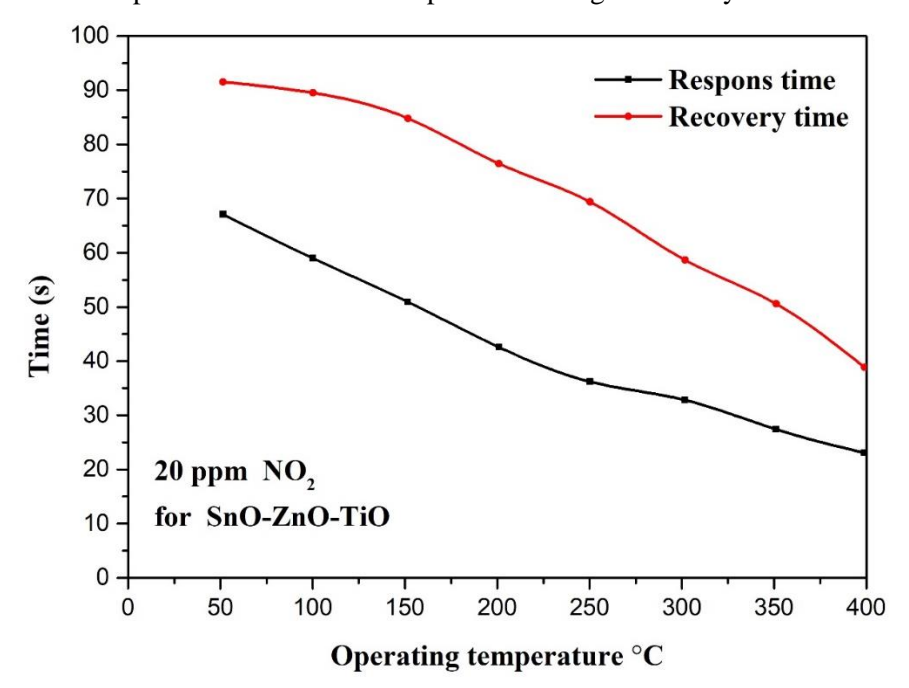


Figure 22 show the relationship between operating temperature with recovery time and response time

4. Conclusion

illustrates the XRD patterns for the synthesized NPs/NCs, showcasing distinct diffraction peaks characteristic of each material. The morphological characteristics of the synthesized NPs/NCs were examined using scanning electron microscopy (SEM). Figure 2 presents SEM images of ZnO, TiO2, and SnO2 NPs, displaying their unique surface structures. ZnO NPs exhibit a rod-like morphology with a uniform distribution, while TiO2 NPs display a spherical morphology with agglomerated particles. SnO2 NPs, meanwhile, showcase a more irregular morphology with scattered particles. The optical properties of the synthesized NPs/NCs were analyzed using UV-Vis spectroscopy. Figure 3 illustrates the UV-Vis spectra for ZnO, TiO2, and SnO2 NPs in the wavelength range of 200-800 nm. ZnO NPs display a prominent absorption peak at around 380 nm, while TiO2 NPs exhibit absorption peaks at 420 nm and 560 nm. SnO2 NPs, on the other hand, demonstrate absorption peaks at 320 nm and 500 nm. These absorption peaks correspond to the band gap energies of the respective materials, indicating their potential for various applications. Gas Sensing Performance Evaluation The gas sensing performance of the synthesized (SnO2/ZnO/TiO2) composite was evaluated using a test chamber setup. The composite material was exposed to varying concentrations of target gases, including NO2, , and the response of the sensor was recorded. Figure 4 illustrates the gas response curves for the composite material towards NO2 Overall, the synthesized (SnO2/ZnO/TiO2) composite exhibited promising gas sensing performance towards NO2 highlighting its potential for environmental monitoring and industrial applications. The structural and optical characterization results further validate the efficacy of the greensynthesis approach utilizing sweet potato Extracted as a reducing agent in producing functional nanomaterials for sensor applications. In conclusion, this study showcases the structural and sensing performance evaluation of a biosynthesized (SnO2/ZnO/TiO2) composite for gas sensor application. The results underscore the potential of green synthesis methods in producing functional nanomaterials with tailored properties for specific applications, paving the way for sustainable and cost-effective sensor technologies in environmental and industrial settings.

References

- 1. N. Hossain et al., "Advances and significances of nanoparticles in semiconductor applications—A review," Results in Engineering, p. 101347, 2023.
- 2. J. Wawrzyniak, "Advancements in improving selectivity of metal oxide semiconductor gas sensors opening new perspectives for their application in food industry," Sensors, vol. 23, no. 23, p. 9548, 2023.
- 3. D. K. Chaudhary, "STUDY ON ELECTRICAL AND OPTICAL PROPERTIES OF ZINC OXIDE SEMICONDUCTOR FOR GAS SENSOR APPLICATION," Amrit Campus, 2023.
- 4. V. V. Petrov et al., "Synthesis, characterization and gas sensing study of ZnO-SnO2 nanocomposite thin films," Chemosensors, vol. 9, no. 6, p. 124, 2021.
- Y. Kong et al., "SnO2 nanostructured materials used as gas sensors for the detection of hazardous and flammable gases: A review," Nano Materials Science, vol. 4, no. 4, pp. 339-350, 2022.
- 6. V. Petrov et al., "Synthesis, Characterization and Gas Sensing Study of ZnO-SnO2 Nanocomposite Thin Films. Chemosensors 2021, 9, 124," ed: s Note: MDPI stays neu-tral with regard to jurisdictional claims in ..., 2021.

- 7. J. Park, I. Lee, and J. Kim, "Physical and Optical Properties of SnO2/ZnO Film Prepared by an RF Magnetron Sputtering Method," Journal of Nanoscience and Nanotechnology, vol. 16, no. 3, pp. 2983-2986, 2016.
- 8. Y.-h. Gui et al., "Enhanced gas sensing properties to NO2 of SnO2/rGO nanocomposites synthesized by microwave-assisted gas-liquid interfacial method," Ceramics International, vol. 44, no. 5, pp. 4900-4907, 2018.
- 9. J. M. Walker, S. A. Akbar, and P. A. Morris, "Synergistic effects in gas sensing semiconducting oxide nano-heterostructures: A review," Sensors and Actuators B: Chemical, vol. 286, pp. 624-640, 2019.
- 10. R. Boppella, P. Manjula, S. Arunkumar, and S. V. Manorama, "Advances in synthesis of nanostructured metal oxides for chemical sensors," Chem Sens, vol. 4, p. 19, 2014.
- 11. W. Chen, Q. Li, L. Xu, and W. Zeng, "Gas Sensing Properties of ZnO–SnO2 Nanostructures," Journal of Nanoscience and Nanotechnology, vol. 15, no. 2, pp. 1245-1252, 2015.
- 12. S. Fakhari, M. Jamzad, and H. Kabiri Fard, "Green synthesis of zinc oxide nanoparticles: a comparison," Green chemistry letters and reviews, vol. 12, no. 1, pp. 19-24, 2019.
- 13. M. Rani and U. Shanker, "Green synthesis of TiO2 and its photocatalytic activity," in Handbook of Smart Photocatalytic Materials: Elsevier, 2020, pp. 11-61.
- 14. L.-L. Li et al., "Room temperature ionic liquids assisted green synthesis of nanocrystalline porous SnO2 and their gas sensor behaviors," Crystal Growth and Design, vol. 8, no. 11, pp. 4165-4172, 2008.
- 15. S. Qiu and S. J. Kalita, "Synthesis, processing and characterization of nanocrystalline titanium dioxide," Materials Science and Engineering: A, vol. 435, pp. 327-332, 2006.
- 16. A. C. Bose, D. Kalpana, P. Thangadurai, and S. Ramasamy, "Synthesis and characterization of nanocrystalline SnO2 and fabrication of lithium cell using nano-SnO2," Journal of power sources, vol. 107, no. 1, pp. 138-141, 2002.
- 17. A. B. Djurišić and Y. H. Leung, "Optical properties of ZnO nanostructures," small, vol. 2, no. 8-9, pp. 944-961, 2006.
- 18. S. Ayed, R. B. Belgacem, J. O. Zayani, and A. Matoussi, "Structural and optical properties of ZnO/TiO2 composites," Superlattices and Microstructures, vol. 91, pp. 118-128, 2016.
- 19. G. Yang, Z. Yan, and T. Xiao, "Preparation and characterization of SnO2/ZnO/TiO2 composite semiconductor with enhanced photocatalytic activity," Applied surface science, vol. 258, no. 22, pp. 8704-8712, 2012.
- 20. W. Maziarz, "TiO2/SnO2 and TiO2/CuO thin film nano-heterostructures as gas sensors," Applied Surface Science, vol. 480, pp. 361-370, 2019.
- 21. B. Lyson-Sypien et al., "Gas sensing properties of TiO2–SnO2 nanomaterials," Sensors and Actuators B: Chemical, vol. 187, pp. 445-454, 2013.
- 22. B. Mondal, J. Das, C. Roychaudhuri, N. Mukharjee, and H. Saha, "Enhanced sensing properties of ZnO-SnO2 based composite type gas sensor," The European Physical Journal Applied Physics, vol. 73, no. 1, p. 10301, 2016.
- Z. Wen and L. Tian-Mo, "Gas-sensing properties of SnO2–TiO2-based sensor for volatile organic compound gas and its sensing mechanism," Physica B: Condensed Matter, vol. 405, no. 5, pp. 1345-1348, 2010.